Exp Fluids (2012) 53:747–763
DOI 10.1007/s00348-012-1325-1

RESEARCH ARTICLE

Vortex dynamics and scalar transport in the wake of a bluff body driven through a steady recirculating flow

Stephane B. Poussou · Michael W. Plesniak

Received: 5 October 2011 / Revised: 1 April 2012 / Accepted: 18 May 2012 / Published online: 5 June 2012

Abstract The air ventilation system in wide-body aircraft cabins provides passengers with a healthy breathing environment. In recent years, the increase in global air traffic has amplified contamination risks by airborne flu-like diseases and terrorist threats involving the onboard release of noxious materials. In particular, passengers moving through a ventilated cabin may transport infectious pathogens in their wake. This paper presents an experimental investigation of the wake produced by a bluff body driven through a steady recirculating flow. Data were obtained in a water facility using particle image velocimetry and planar laser induced fluorescence. Ventilation attenuated the downward convection of counter-rotating vortices produced near the free-end corners of the body and decoupled the downwash mechanism from forward entrainment, creating stagnant contaminant regions.

1 Introduction

This paper presents an experimental investigation of a bluff body wake moving at moderate Reynolds number ($Re_D = 9{,}600$, based on body width, D) through a flow pattern steadily recirculating in a semi-circular enclosure. This ventilation flow is characteristic of a Boeing 767-300 aircraft. Such flow interaction was reported to produce strongly three-dimensional, transient velocity fields (Poussou 2008). This work contributes to the understanding of contaminant transport in human wakes moving through ventilated aircraft cabins, in the context of breathing air quality and passenger safety (Poussou et al. 2010). As a typical contaminant dispersion scenario, a person is assumed to walk along the central aisle of a ventilated cabin during flight. At a particular point in time, the individual releases an airborne contaminant (e.g. virus by sneezing) that propagates in the cabin, as shown in Fig. 1. From a sanitary perspective, it is desirable to quantify the distance over which contamination is possible, as well as the number of seat rows and passengers that may need decontamination or medical attention. Numerical simulation of such convoluted transient flow phenomena is difficult because of the spatial and temporal scales involved, and actual experiments on contaminant distribution in real cabins are often impractical. More generally, the prediction of contaminant dispersion in indoor environments is a complex problem involving heating, ventilation, and air-conditioning phenomena, which may interact with short-term unsteady flows created through human motion. Further understanding of these transport mechanisms is needed to properly evaluate dispersion risks and optimize decontamination procedures. The present study contributes to the refinement of numerical models aiding the design of ventilation systems and air monitoring procedures in the commercial aircraft industry. Additional applications may be found in engineering (mass transportation systems, pollutant transport behind vehicles in tunnels, pollution downstream of buildings), medical environments (hospitals, operating rooms), public security (biochemical warfare, transportation), or industry (clean rooms, pharmaceutical production, toxic wastes).

S. B. Poussou
School of Mechanical Engineering, Purdue University, West Lafayette, IN 47907, USA

M. W. Plesniak (✉)
Department of Mechanical and Aerospace Engineering, The George Washington University, 801 22nd Street, N.W., Washington, DC 20052, USA
e-mail: plesniak@gwu.edu

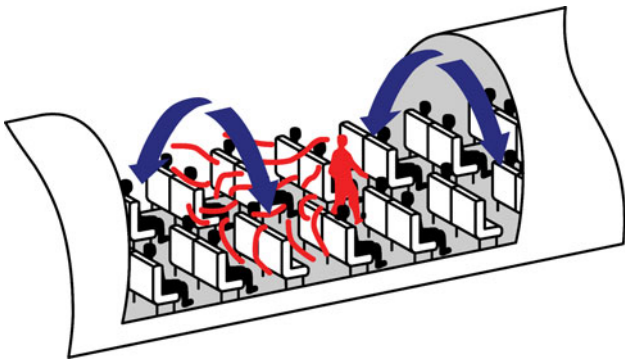

Fig. 1 Schematic representation of contaminant dispersion in the wake of an individual walking through a ventilated aircraft cabin

1.1 Cabin airflow and contamination in aircraft

In commercial wide-body jetliners, a controlled amount of outside air is continuously added to the cabin via the environmental control system. Unlike office spaces, this indoor environment is characterized by large quantities of air entering a relatively low volume cabin, a high occupant density, extended periods of breathing exposure, and separate ventilation zones (flight deck, galley, lavatory, cabin, etc.) Precise control of the ventilation airflow pattern is therefore required to distribute and circulate air adequately in the cabin, since passenger perception may be focused on temperature gradients (cold regions), air velocity fluctuations, and ambient air quality (stagnant air, odors), among others. For example, specifications for the Airbus A330/A340 aircraft family require air velocities to be less than 0.25 m/s in the seat area, and temperature layer differences to be smaller than 3.5 °C (Müller et al. 1997). In the main cabin, air is typically supplied from overhead distribution outlets running the length of the cabin; these outlets are carefully designed to produce circular airflow patterns. The air is continuously exhausted through sidewall linear grilles at floor level. The ventilation system produces two-dimensional flow, so that air supplied at one seat row leaves approximately at the same seat row, in order to minimize net airflow along the cabin length and spreading passenger-generated contaminants. Although flow rates entering and leaving the cabin are matched to minimize net longitudinal flow, fluctuating velocity components of the order of 0.1–0.3 m/s have been observed and deviation from symmetric flow has been reported (Mo et al. 2003). A comprehensive technical overview of aircraft ventilation is available in the literature (National Research Council 2002).

In order to evaluate the risks associated with airborne contamination, knowledge of the fluid mechanics governing the airflow is necessary. A survey of the literature reveals a dearth of information on cabin flows in the public literature, which may be attributed to proprietary aircraft cabin designs, as well as the specificity and uniqueness of associated ventilation airflows. Experimental studies in actual cabins or scaled mockups have limitations in measuring tracer concentration or velocity fields. Large-scale flow features combined with relatively low velocity magnitudes pose substantial challenges for data processing algorithms, camera resolution, flow field illumination, particle seeding, and velocity boundary conditions. Consequently, numerical simulations have been traditionally preferred because they allow control of flow conditions and more efficient variation of a wide range of parameters, such as internal geometrical obstructions (seats, passengers), thermal effects (cooling jet, heated passengers) or modes of contaminant dispersion (initially present or released by passengers). The first comprehensive study of the effect of cabin airflow on contaminant dispersion was conducted by Mizuno and Warfield (1992). Müller et al. (1997) investigated the isothermal flow in a full-scale Airbus A330/A340 cabin mockup equipped with seats. Their pioneering use of helium-filled bubbles as seeding particles for particle tracking velocimetry (PTV) opened the door to quantitative measurements of large-volume, low-speed airflows, which could not be achieved by traditional flow measurements techniques, such as particle image velocimetry (PIV), PTV, laser Doppler velocimetry, or hotwire anemometry. Mo et al. (2003) used conventional PIV to investigate the flow field in an actual Boeing 737 cabin with seats and heated mannequins and to provide validation data for computational fluid dynamics (CFD) models. Sonic anemometry was used by Garner et al. (2004) for CFD validation of a very low (2–5) air-exchange per hour airflow, in which incoming flow remained attached to the luggage bin due to the Coanda effect. The helium bubbles technique was further extended to volumetric particle streak velocimetry (VPSV) by Sun et al. (2005), Zhang et al. (2005), and Wang et al. (2005). They investigated the effect of obstructions and cold incoming flow in an actual Boeing 767 cabin furnished with seated isothermal mannequins. They found that obstructions affected significantly the velocity field at passenger breathing level. They recommended further investigation of the effect of localized disturbances on the cabin airflow and contaminant dispersion, such as passenger and crew movement. Bosbach et al. (2006) used PIV to study the incoming jet along the idealized luggage compartment in an Airbus A380 full-scale cabin. Wang et al. (2006, 2008) used CO_2 concentration to estimate the local mean age of air and evaluate ventilation performance. The influence of thermal conditions on the flow field was further studied by Kühn et al. (2008) in an Airbus A380 mockup.

Numerical simulations have explored in greater details the influence of cabin flow parameters. Aboosaidi et al. (1991) used Reynolds-averaged Navier-Stokes (RANS) simulation to estimate the performance of inlet diffuser

designs. Singh et al. (2002) conducted a steady RANS simulation using the Re-Normalization Group (RNG) $k-\epsilon$ model, with and without occupants and their corresponding heat loads. Higher mixing was observed in the regions close to passengers sitting nearer the aisle than the window, where regions of higher velocity and temperature gradients were reported. CFD simulation was further used by Zhang and Chen (2007b) and Gao and Niu (2008) to assess the performance of novel cabin ventilation systems, showing that personalized ventilation offered the best level of protection against draft. Recently, a number of studies have focused on cabin airflow (Liu et al. 2012) and contaminant migration (Yan et al. 2009; Mazumdar et al. 2011), origin detection (Mazumdar and Chen 2008; Zhang and Chen 2007a; Zhang et al. 2007, 2009) and decontamination (Baker et al. 2006, 2008), in an effort to facilitate treatment of victims in a timely manner, optimize cabin decontamination and decrease the financial cost of grounded airplanes.

Air quality in aircraft has been the subject of continued investigations (Nagda et al. 1992; Dechow et al. 1997; McKernan et al. 2008), with a renewed interest since the global outbreak of severe acute respiratory syndrome (SARS) in 2003 (Spengler and Wilson 2003). Although a comprehensive assessment of the cabin environment by the NRC (2002) concluded that aircraft ventilation systems do not appear to enhance infectious transmission, cases of disease outbreaks onboard have been documented in numerous epidemiologic studies of international scale (Mangili and Gendreau, 2005). Although large-scale numerical models have been developed to predict airborne particle dispersion and deposition (Gao and Niu 2007), distribution (Lai et al. 2008), and contamination in indoor environments (Chen et al. 2006), the underlying turbulent dispersion is an intensive field of research. Droplet nuclei can remain suspended for prolonged periods of time before inhalation and retention in the respiratory tract, in quiescent air or when the exhaust flow rate is insufficient. Because most viruses and bacteria have a short life expectancy or growth, it is crucial to determine particle migration shortly after emission. In particular, particles may accumulate at high contagious concentration level within transient turbulent eddies. Risks associated with airborne infection depend on several factors: the presence of an infectious person effectively releasing infectious agents, ventilation flow rate, mixing of cabin air, proximity to the infected source person, duration of exposure, and infectious power of the agents. As reviewed by the NRC (2002), virulent outbreak cases have involved SARS, influenza, varicella, measles and West Nile virus, while bacterial contagion have been reported for diphtheria, pertussis, pneumonia, meningococcal disease, and tuberculosis. Kenyon et al. (1996) provided evidence for transmission of tuberculosis from an index patient to other passengers seated in adjacent rows in the same section. However, transmission scenarios and infection routes are usually difficult to identify because outbreaks can be simply triggered by poor or absent ventilation (Moser et al. 1979), and interpretation of post-flight medical testing data is often statistically inconclusive (Wang 2000; Zitter et al. 2002). Other epidemiologic studies reported that sufficient exposure occurs only to persons seated next to the infected source person, suggesting that droplet nuclei are well captured by the ventilation air flow. In support of this view, Wick and Irvine (1995) measured higher bacteria concentrations near the floor exhausts compared to breathing levels of seated passengers, confirming that air streams play a major role in contaminant migration in the cabin. However, it is not clear how much flow disturbance along the aisle can contribute to spread infection, especially when ventilation is not operated at maximal flow rate. Olsen et al. (2003) reported indeed a case of transmission of SARS on a 3-h flight carrying 120 passengers, of which at least 22 people were infected while seated 7 rows in front and 5 rows behind the index passenger. No scenario could be clearly identified, as the incident might have been caused by airborne transmission, filter malfunction, and pre- or post-flight infection.

1.2 Wake dynamics in finite bluff body flows

Although the geometry of the human body varies in dimensions and small-scale details, the flow around it can be idealized as a finite bluff body flow. Such flow is characterized by persistent vortex shedding, a large region of separated flow, and a high coefficient of drag comprised of pressure drag. Finite bodies in uniform cross flow over a ground plane are typically classified via the aspect ratio, $AR = H/D$, which compares body height, H, to span, D (body diameter or width depending if the base is circular or rectangular). In a very elongated body ($AR \rightarrow \infty$), the flow resembles that of an infinite cylinder (Williamson 1996; Roshko 1993), in which the ends are so remote that they do not influence the flow. As AR approaches 1, the flow from the free-end starts to interact with vortex shedding from the sides and the flow departs from two-dimensionality. Furthermore, as AR tends to 0, vortex shedding from the free-end is predominant and the flow eventually approaches the flow over a step wall. A generic human body of 1.74 m (68.5 in) height and 0.58 m (22.8 in) width may be represented by a finite cylinder mounted on a ground plane with $AR = 3$, where the three-dimensional flow from the head and shoulders interacts with vortex shedding from the lateral sides. Its aerodynamic human wake has a typical Reynolds number of 5×10^4 at a walking speed of 1 m/s, which corresponds to the subcritical regime (Roshko 1993).

The literature on finite bodies in uniform cross flow is extensive, due to their relevance to unsteady flow patterns of importance to civil engineering (grain stacks, cooling towers, bridge piles), or mechanical engineering (flame holders in combustion chambers, vibrating cantilevers, landing gears). There has been considerable work done on stationary cylinders mounted on a ground plane in uniform flow and immersed in its boundary layer. The flow typically comprises three components: (a) a three-dimensional horseshoe vortex system near the base, (b) a two-dimensional Kármán-type vortex shedding along most of the cylinder height, and (c) a three-dimensional separated flow over the free-end.

Sumner et al. (2004) conducted a comprehensive review of flows around circular cylinders. The effect induced by both cylinder extremities on the near-wake was investigated by Park and Lee (2000, 2004), who obtained detailed measurements of the flow separation over the free-end. Their observations were consistent with the observations reported by Tanaka and Murata (1999). The flow field in the near-wake (mean velocity and vorticity) was measured by Sumner et al. (2004), with particular attention given to tip vortices. Cylinders with $AR = 3$ had a wake structure distinctly different from those with $AR = 5, 7, 9$, in which a secondary vortex pair was found near the cylinder-ground junction. The effect of the aspect ratio on vortex shedding and three-dimensionality was studied by a large number of authors. Farivar (1981) obtained vortex shedding frequencies for cylinders of aspect ratio $2.8 < AR < 15$. Shedding frequencies measured by Okamoto and Yagita (1973) showed that the Strouhal number progressively decreased as one approached the tip. Sakamoto and Arie (1983) included the effect of the boundary layer developing on the ground plane in their study of circular and rectangular cylinders in the laminar regime. Their results revealed that the aspect ratio controlled the type of vortices produced in the wake, depending on a critical value: (a) symmetric, arch-type vortices at a definite frequency for $AR < 2$ (rectangular) and $AR < 2.5$ (circular), or (b) asymmetric, Kármán-type vortices for aspect ratios $AR > 2.5$. The large eddy simulations (LES) by Afgan et al. (2007) agreed with the experimental data from Park and Lee (2002). The effect of non-circular cylinders has been studied by a limited number of authors. Martinuzzi and Tropea (1993) observed arch-type shedding in the near-wake of a cube. Song and He (1993) used LES to obtain the velocity and vorticity fields behind a rectangular cylinder at $AR = 4.7$, and reported that the vortex shedding frequency from the free-end was twice that of Kármán vortex shedding. Huber et al. (1991) obtained smoke dispersion measurements from a point source located upstream of the body. In summary, circular cylinders of finite height mounted on a ground plane generate complex and strongly three-dimensional wakes. The flow over the free-end produces a pair of counter-rotating vortices persisting in the streamwise direction of the wake (Kawamura et al. 1984; Park and Lee 2000, 2002, 2004; Sumner et al. 2004). The resulting downwash interacts with Kármán vortex shedding from the sides of the cylinder, and may prevent roll-up of the shear layer. Depending on the aspect ratio, the downwash may alter the location of the boundary layer separation point on the cylinder surface, the shedding frequency, and back pressure in the wake. When the aspect ratio is smaller than a critical value (varying between 1 and 7 due to non-homogeneous experimental conditions), the downwash may annihilate completely antisymmetric Kármán vortex shedding and promote symmetric arch-type vortex shedding at one frequency (Kawamura et al. 1984; Taniguchi et al. 1981a, b; Fröhlich and Rodi 2004; Sakamoto and Arie 1983; Okamoto and Sunabashiri 1992; Tanaka and Murata 1999) until the pair of longitudinal tip vortices eventually no longer exists. The literature provides relatively few experimental studies of low-aspect-ratio circular or rectangular cylinders, with incomplete or fragmented description of the flow field. While the mean velocity field for low AR is well documented (Tanaka and Murata 1999; Sumner et al. 2004), the turbulent quantities necessary to understand wake transport are either restricted to a limited number of measurement planes (Okamoto and Sunabashiri 1992) or regions very near to the cylinder (Park and Lee 2004). It is worth noting that a variety of flow interactions with cylinder wakes has been investigated. They include influence of shear (Saha et al. 2001), side-by-side cylinder configuration (Kolar et al. 1997), or presence of a nearby wall (Liou et al. 2002). In particular, Wolochuk et al. (1996) studied the effect of shear and high freestream turbulence on vortex shedding and unsteadiness from bluff bodies. Although these flow interaction phenomena contribute to contamination dispersion in a real scenario, they are not discussed herein and are beyond the scope of the present study.

Stationary bodies in uniform flow have been well documented for their prevalence in modeling wind load on buildings or worker exposure to hazardous airborne substances. In the case of buildings applications, it is usually important to capture the effect of the approaching atmospheric boundary layer. Such studies have benefited from the experimental ease and flow control options offered by wind or water tunnels. On the other hand, bodies self-propelled or driven through a quiescent fluid have been studied to a lesser extent, because of the challenges they pose for modeling and experimenting. A complete understanding of the formation and development of their vortex structures is presently lacking, although data exist on self-propelled slender bodies (Thomas et al. 1991). Interpretations drawn from one type of flow extended to another

require caution, for the presence of an approaching turbulent boundary layer over the ground plane induces different flow physics in the wake. As pointed out by Sakamoto and Arie (1983), an adverse pressure gradient develops near the base of a stationary finite body because of flow deflection around the obstruction (Doligalski et al. 1994). To the best knowledge of the authors, only one publication by Slaouti and Gerrard (1981) reported on the wake of a finite body moving in a quiescent fluid, i.e. without boundary layer and junction flow. They obtained flow visualization for a cylinder towed in a water tank at uniform speed and low Reynolds number and varied the end configurations (free-end, free surface, attached plate) and cylinder configurations (aspect ratio, yaw). Their results are not directly applicable to finite bodies, as they focused on the flow region near the end of a high-aspect-ratio cylinder ($AR \approx 25$) and do not provide insight on the wake at the base in the absence of boundary layer. Also, the ground plane was too far from the tip for any downwash to develop. However, flow visualization revealed that a portion of cylinder 3 or 4 diameters long from the tip inhibited vortex shedding in its near-wake, which gradually contracted downstream due to mixing. The rest of the cylinder was not affected by end effects and the flow resembled that of an infinite cylinder.

While wakes behind bluff bodies have been the subject of extensive research, it is only relatively recently that efforts have been reported for the flow around a realistic human body, based on morphological details and body kinematics. Numerical simulations have been used as a primary, but limited, tool of investigation, due to the challenges of large scales involved, and combination of three-dimensional transient flow features and flow excitations emanating from moving boundaries (Chen et al. 2010). The recent availability of high-performance computing resources has allowed using the LES technique over RANS for such flows, because RANS models have difficulties in predicting separation behind bluff bodies (Lakehal and Rodi 1997; Lübcke et al. 2001; Richmond-Bryant et al. 2006). However, RANS models are still predominant among human exposure studies in the indoor air community as they are readily available in commercial CFD packages and computationally inexpensive. While most studies have focused on the human thermal flow and drag (Murakami et al. 1999), a limited number of authors have studied the dynamics of a human wake standing in a uniform flow of constant freestream velocity. Kim and Flynn (1991) observed experimentally a strong downwash above chest level for an isothermal mannequin. Kulmala et al. (1996) found a mean recirculation length of 1.5 diameter behind a mannequin, which depended little on the freestream velocity. Edge et al. (2005) confirmed by RANS the existence of a recirculation region behind the torso, contributed by asymmetric vortex shedding. The downwash produced lateral expansion of the lower portion of the wake. Their measurements suggested the presence of large-scale structures advecting up to five diameters downstream. Choi and Edwards (2008) introduced the use of a human kinematics model in LES and were able to simulate a person walking indoors and transporting contaminant. They showed that contaminant was transported over a distance of 8 m (26 ft) in full-scale, and that even after the person stopped, inertial effects could keep the contaminant convecting forward. Donnert et al. (2007) injected a tracer substance upstream of cylinders at various elevations and were able to obtain concentration maps in horizontal planes. Overall, the literature on scalar transport in wakes behind cylindrical bluff bodies is limited, especially for experiments in water.

In summary, there is a lack of necessary experimental data reported in the literature to support the investigation of contaminant spreading in an aircraft cabin due to a human wake, more specifically of the flow dynamics in the wake of a bluff body driven through an ambient recirculating flow typical of an aircraft ventilation flow pattern. Although the cabin airflow, the human wake and airborne particle transport have all been studied individually, their interaction in a dynamic configuration is not understood despite their alleged role in respiratory illness outbreaks. On one hand, it is believed that the air circulation pattern has little net flow in the longitudinal direction and that the risk of infection from a contagious passenger to another passenger is limited to close range, i.e. one seat row. On the other hand, a growing body of experimental and numerical evidence suggests that localized disturbances have potential to impact the contamination process at the temporal and spatial scales of the cabin airflow. An experimental study is needed to address the problem from a fundamental perspective. It is hypothesized herein that the effect of ventilation is to elevate the wake from the floor and promote longitudinal spreading of contaminant. The goal of the present study is to contribute experimental data for the transient flow interaction and provide an understanding of its implication for scalar migration in the context of aircraft disease contamination. In particular, the following objectives are addressed in this study: (a) characterize the evolution of the vortex pair responsible for the downwash downstream of the body under ventilated conditions; (b) measure convective scalar transport in the wake; (c) identify basic fluid flow mechanisms governing the interaction between the wake and the recirculating flow.

2 Modeling approach and assumptions

Indoor environments involve heat and mass transfer phenomena introduced by flow interactions between the

ventilation, occupants and stationary objects. Aircraft cabins have even more complex environments due to the presence of thermal gradients (walls, ventilation jets, passengers), high mixing ratios, and complicated spatial geometries (cabin configuration, moving obstacles), all of which may be combined with variable ventilation schemes. These flow conditions are challenging for full-scale experimental investigations, raising difficulties such as financial cost, time constraints, insufficient control of flow and thermal conditions, or poor spatial and temporal resolutions. In addition, random motions and behaviors of seated and moving passengers further complicate the flow field. In order to focus on fundamental flow mechanisms governing the interaction between the recirculating flow and a moving wake, the present experiment used an idealized, scaled (1:10) cabin geometry representative of a Boeing 767-300. The cabin model was chosen as an empty, semi-cylinder; an elaborate reproduction of an actual aircraft cabin would bring little scientific value since results would be contingent on specific (often proprietary) designs and would lack comparative reference data. In the present study, the bluff body modeling a moving person was chosen to translate along the central aisle, because body motion within a side aisle would resemble the classical and well-studied problem of a body moving in a cross flow. Instead, the central aisle produces a unique configuration where the body moves through the region where ventilation flows collide and counteract the descending convection of the wake, which has not been previously studied, to the best knowledge of the authors. Such flow combination is hypothesized to lift the wake and increase the residence time of contaminants in the ventilated cabin by opposing the purging effect of the ventilation pattern, therefore promoting contamination.

In order to reduce the number of variables, idealized geometries and kinematics were assumed. To first approximation, the human body may be represented by a circular cylinder or an arrangement of cylinders (Edge et al. 2005). There is a vast amount of data on finite circular or elliptical cylinders available in the literature for comparison. However, a parallelepiped was chosen for experimental reasons: square edges lock flow separation points at the leading edge unlike in the case of a cylinder, where downstream wake characteristics are strongly dependent on flow separation (Kawamura et al. 1984). Moreover, locked separation points facilitate boundary conditions in CFD simulations, especially as the RANS $k-\epsilon$ model is known to delay boundary layer separation for a circular cylinder (Flynn and Eisner 2004). The cabin interior consisted of an empty semi-cylinder separated from the floor by a slotted opening on side walls to permit exhaust of ambient fluid. Atop the cabin, an inlet nozzle consisted of a continuous linear slot running along the entire cabin length and supplying fluid in the tangential direction. The motion of the body was assumed linear and steady to avoid inertial effects that were not the primary focus of this investigation. The flow was assumed to be at constant temperature and only isothermal fluid flow phenomena were investigated. Buoyancy effects (e.g. cooling jet) and the human thermal plume (Craven and Settles 2006) were beyond the scope of the study to focus on governing fluid mechanisms and to provide validation data for CFD isothermal models, which may in turn be incrementally used and validated as experimental tools to investigate thermal effects and other full-scale details neglected in this fundamental study. Due to practical limitations with the frequency of the imaging system used in the experiments, a full-scale velocity of 0.25 m/s in air was used in this model instead of 1 m/s, which is the typical speed of a walking person. Although lower, such velocity allowed (a) capturing the underlying flow physics while providing sufficient spatial and temporal resolutions in the near wake, since the human aerodynamic wake has been shown to replace the human thermal plume above 0.2 m/s (Edge et al. 2005), and (b) representing cases in which people move slowly in a line, cabin crew slowly push a cart, or passengers walk with difficulty. Furthermore, buoyancy effects were not present in this study and thus did not affect wake development in this lower velocity range. Details on similarity analysis and model scaling are provided by Poussou (2008) and Mazumdar et al. (2011), and summarized in Table 1 and Fig. 2.

3 Experimental setup and procedure

3.1 Flow facility and control system

The experiments were performed in a closed-loop test facility utilizing 2.6 m^3 (700 gal) of recirculating water.

Table 1 Model parameters at ambient temperature (20 °C)

Parameter	Full-scale	Model-scale
t (cm)	23.2	2.2
D (cm)	58	5.54
H (cm)	174	16.6
U_{body} (m/s)	0.25	0.175
U_{vent} (m/s)	0.765	0.175
d_{cabin} (m)	4.72	0.45
L_{cabin} (m)	25.5	2.44
h (mm)	10	0.1
Q (L/s/row)	13.1	0.084
v (m^2/s)	1.5×10^{-5}	1.01×10^{-6}
$Re_D = U_{body}D/v$	9,670	9,600

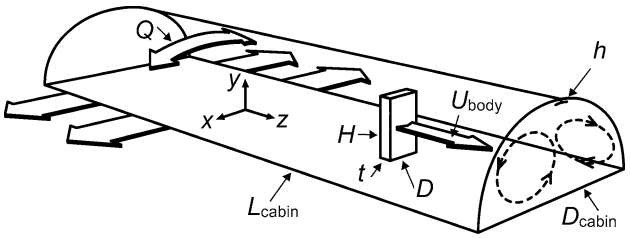

Fig. 2 Problem geometry and dimensional variables

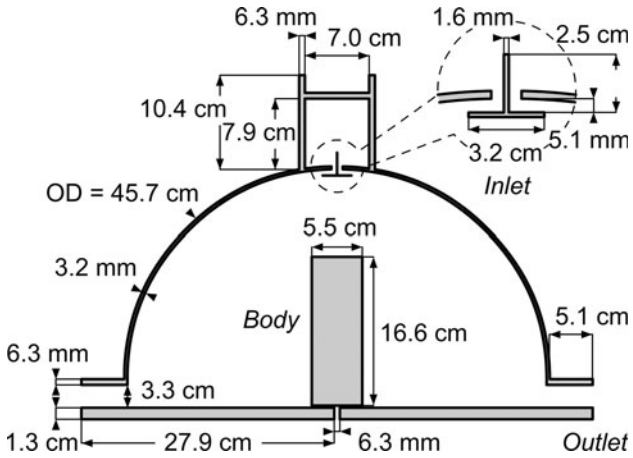

Fig. 3 Geometry and dimensions of the cabin, bluff body, and inlet diffuser

The cabin was fully submerged in an optical index-matching, glass tank measuring 94 × 94 × 244 cm (550 gal capacity). Guidelines by Budwig (1994) were used for the index matching procedure. Visual access was possible from all sides. The cabin model consisted of an optically-clear, semi-cylindrical acrylic duct of 45.1 cm inner diameter, 244 cm length and 3 mm wall thickness; cross-sectional dimensions are provided in Fig. 3. In particular, the cabin was inverted (i.e. upside-down) to take advantage of the isothermal nature of the study (i.e. no buoyancy effects) and allow the body motion system to be located outside of the water for practical reasons. Water (ventilation flow) entered the cabin via a set of manifolds leading to a settling chamber designed to reduce fluctuations, after which a longitudinal, T-shaped diffuser (5 mm wide slot) produced uniform, tangential injection of water into the cabin in the form of two planar jets. Water exited the cabin through 3.3 cm wide slots located at floor level on each sidewall of the cabin. Flow was driven by a 1.1 kW (1.5 hp) primary pump producing a flow of up to 285 L/min (75 gal/min) into the cabin, and a secondary filter pump returning water to a 0.6 m^3 (150 gal) reservoir. The flow rate through the cabin was measured with a nonintrusive ultrasonic flow meter (GE Panametrics TransPort PT878).

The bluff body consisted of an acrylic, smooth, square-edged parallelepiped measuring 16.6 × 5.54 × 2.23 cm,

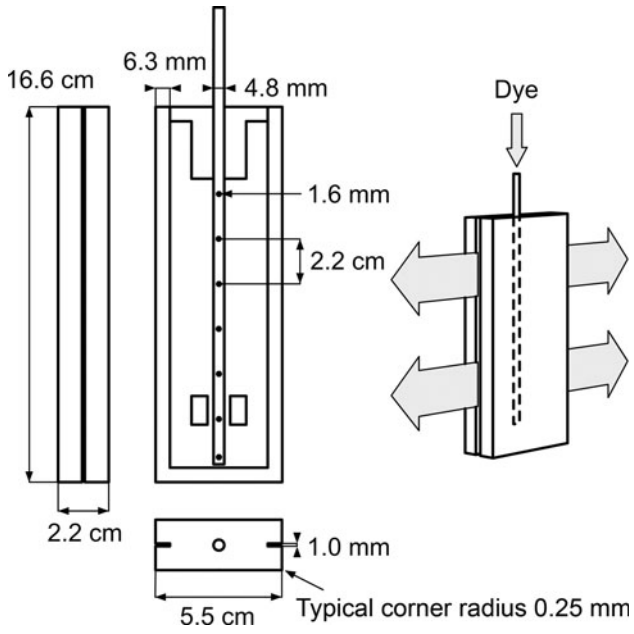

Fig. 4 Geometry and dimensions of the bluff body, showing dye injection

as shown in Fig. 4. A gap separated the front and rear parts constituting the body, and permitted injection of fluorescent dye laterally from the sides of the body for flow visualization. The gap width (1 mm) was of same order of magnitude as the thickness of the laminar boundary layer developing on the sides of the body ($\delta = 0.9$ mm, calculated using a parabolic velocity profile). Such gap size prevented the flow of dye from significantly disturbing wake characteristics and downstream flow development. The boundary layer containing the dye was calculated to be laminar over the sides of the bluff body at $Re_D = 9{,}600$. The dye entered a flow conditioning cavity inside the body via a 6.3 mm diameter stainless steel tube, which also served to drive the body.

Body translation to simulate a walking passenger was achieved using a stepper motor (Oriental Motor PK268M-03A) located above the water. The motor was installed on a cart rolling along a traverse system above the submerged cabin floor. A vinyl belt sliding longitudinally with the body was used to seal the slot along the cabin floor, and thus prevented undesired flow of water through the slot. A digital motor controller (Velmex VXM 3.25) and an optical incremental encoder disk (US Digital E5D-360-250) were used for position and speed control. The motion system was integrated to a data acquisition system controlled by a personal computer (Dell OptiPlex GX260, CPU 1.8 MHz, RAM 512 Mb). A custom-built virtual instrument written in LabVIEW 8.0 software (National Instruments) acted as a time master interface to synchronize the laser diagnostic system with body motion. Additional information about the setup and its operation can be found in Poussou (2008).

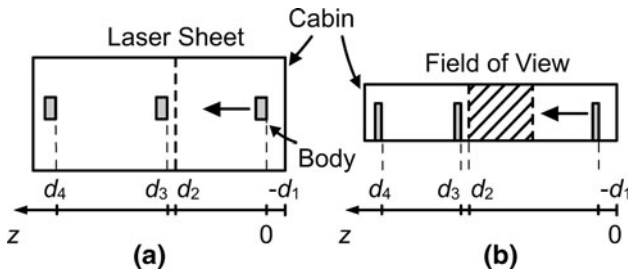

Fig. 5 Experimental configuration for **a** end-view and **b** side-view measurements

Table 2 Geometrical configuration for optical measurements ($D = 5.54$ cm)

	End-view		Side-view	
	(a)	(b)	(a)	(b)
d_1	3.0D	1.7D	3.0D	1.7D
d_2	15.1D	6.2D	18.6D	11.6D
d_3	15.3D	6.4D	18.7D	11.6D
d_4	29.1D	22.7D	32.7D	22.7D

One general objective of the present study is to assess the impact of wake transport on seated passenger contamination, i.e. the time evolution of contaminant concentration at fixed locations in the cabin, and more specifically on lateral spreading in the cabin. Therefore, the optical configuration was chosen to measure wake decay in planes at fixed locations in the cabin, instead of obtaining data in a moving reference frame relative to the body. Two experimental configurations (referred to as end-view for cross-sectional data, and side-view for longitudinal data) were used to characterize the flow, as shown in Fig. 5, and summarized in Table 2. For each experimental run, the back face of the body was placed against the cabin interior wall at a distance d_1 from the origin ($z/D = 0$); this distance was chosen to minimize end effects. Starting from $z/D = 0$, the body was translated along the cabin centerline at a constant speed corresponding to $Re_D = 9{,}600$. Sequential measurements were taken within the illuminated field of view (cross-sectional or lateral) as soon as the back face of the body reached d_3. The body traveled to d_4 before being returned to its original position. The non-zero distance $d_3 - d_2$ prevented potential physical damage to the digital camera from excessive reflection of light at the surface of the body.

3.2 Particle image velocimetry (PIV) setup

Velocity measurements were made using a commercial PIV system (TSI). The laser sheet was produced by a dual 5 ns pulse, frequency-doubled 532 nm Nd:YAG laser (New Wave, Gemini PIV) capable of 50 mJ per pulse. Images were recorded using a fast interline transfer, 2,048 × 2,048 pixels, 12 bit gray levels digital camera (TSI, PowerView 4MP), controlled by a synchronizer (TSI, LaserPulse) and a data acquisition computer (Dell T3400 2.4 GHz Dual Core, 2 Gb RAM). A commercial software (TSI, Insight 3G v8.0.5) was used to correlate images. Images were typically analyzed using a multiple-pass recursive Nyquist grid of initial size 64 × 64 pixels and final size 32 × 32 pixels. A fast Fourier transform (FFT) based cross-correlation algorithm was employed without masking, as well as a Gaussian subpixel interpolation scheme and a central difference algorithm for calculation of the velocity. For cases with weak correlation, direct correlation was employed instead of FFT correlation, at the expense of computational time. The time interval between two successive laser pulses was typically between 1,500 and 2,500 μs when making cross-sectional measurements, which minimized the number of particles unmatched between two images due to out-of-plane motion, and appropriately minimized noise in the correlation function. A mean filter was employed to validate the instantaneous velocity fields and remove spurious vectors. The vector density was typically of 44 vectors/cm^2, with a 50 % interrogation window overlap. Silver-coated hollow glass spheres (Potters Industries, Conduct-O-Fil SH400S33) were used for particle seeding. These particles had a mean diameter of 14 μm and a specific gravity between 1.6 and 1.7. Under typical experimental conditions, the particle Stokes number was of the order of 0.01 and thus could be considered as passive tracers in the flow.

For the baseline wake flow without ventilation, the bluff body moved through the fixed, cross-sectional measurement plane, and a series of 30 consecutive PIV images were captured to obtain transient (x, y) velocity fields of the wake at a spatial resolution of 3.8 × 3.8 mm in physical space. Phase-averaged velocity fields at planes of same z/D values were obtained by repeating the body motion 105 times, which was sufficient for convergence of the low-order derivative quantities. The relatively low number of ensembles was due to experimental limitations, such as motor heat-up. Between each motion event, the body was kept still for a prolonged period (typically 2 min) to allow the ambient fluid to reach steady state. The body moved at a speed of $U_{\text{body}} = 0.175$ m/s in model-scale (water), equivalent to 0.25 m/s in full-scale (air); the corresponding Reynolds number was $Re_D = 9{,}600$. The double-pulsed laser was operated at a repetition rate of 7.25 Hz ($\Delta t = 138$ ms) with a time interval of 2,000 μs between pulses, resulting in longitudinal spacing of $\Delta z = 24.1$ mm, i.e. $\Delta z/D = 0.43$. Measurements planes were acquired in the range $0.18 < z/D < 12.82$ ($0 < t/T < 12.64$), where the

characteristic time is defined by $T = D/U_{body}$. The equivalence between z/D locations and t/T times is given by $t/T = (n - 1) \times 0.44$ and $z/D = 0.181 + (n - 1) \times 0.436$, where n denotes the frame number. For the interaction wake flow with ventilation, the PIV system captured 201 repetitions of body motion each including 30 consecutive PIV images at a 5.3 × 5.3 mm spatial resolution in physical space. The double-pulsed laser was operated at the same repetition rate. The body moved at a speed of $U_{body} = 0.175$ m/s ($Re_D = 9{,}600$) and ambient fluid in the cabin was recirculated at a steady flow rate $Q = 2.5$ L/s ($Re_h = 500$), corresponding to 40 air cabin exchanges per hour in full-scale.

3.3 Planar laser induced fluorescence (PLIF) setup

Fluorescein sodium salt $C_{20}H_{10}O_5{\cdot}2Na$ (also referred to as disodium salt or uranine) was chosen as fluorescent dye for flow visualization and illuminated with the same Nd:YAG laser used for PIV. As reported by Karasso and Mungal (1997), the absorbance of sodium fluorescein at the 532 nm excitation line is very low, thus requiring high laser intensity. In addition, sodium fluorescein has a non-linear signal response when excited by the Nd:YAG laser, which restricts the use of this laser/dye combination to purely visualization purposes. The salt was dissolved in water at concentrations larger than 50 ppm to allow acceptable imaging. The temperature of the dye was monitored and controlled to match the temperature of the water in the closed-loop facility, in order to avoid buoyancy effects. The dye was contained in a 20 L vessel fed pressurized by air at 7 psig, which delivered dye to the bluff body at a 25 mL/s flow rate. Upon injection into the flow, the dye was illuminated by the laser sheet (approximately 1 mm thick) and recorded by a video camera (Canon, PowerShot G7) at a frequency of 15 frames per second and a 1,024 × 768 pixels resolution. It was verified that the experimental setup produced uniform injection from both sides of the body.

3.4 Experimental uncertainty

The experimental setup introduced fixed errors through the motion system (displacement increments) and monitoring instrumentation (flow meter). Under typical operating conditions, the relative uncertainty associated with U_{body} was estimated to be less than ±1 %, and less than ±4 % for the cabin water (ventilation) volumetric flow rate, Q. The PIV technique introduced fixed errors through post-processing. The relative bias uncertainty in particle displacement was estimated to be less than ±4 % when using subpixel detection schemes. Random errors associated with mean flow velocity measurements were estimated statistically. Pixel displacement errors were combined with processing errors at a 95 % confidence interval (Moffat 1988). For a typical ensemble of 100 instantaneous PIV realizations, the total relative uncertainty in the phase-averaged velocity was estimated to be less than ±5 % in both directions within the plane of measurement. Due to out-of-plane particle motions arising from three-dimensionality, a small fraction of vectors (less than 5 %) was discarded using filtering methods. Details on the uncertainty analysis are available in Poussou (2008).

4 Results and discussion

4.1 Evolution of the free-end vortex pair

Cross-sectional, phase-averaged (x, y) velocity fields were acquired at various z/D downstream distances from the body. For reference, the velocity field corresponding to the transient downwash flow typically observed downstream of this bluff body was studied using PIV by Poussou (2008) and is illustrated in Fig. 6, where the vortex pair produced by the free-end corners (shoulders) convects in the downward direction. In the present study, the path followed by vortex cores was obtained by tracking the centers of curvature of the associated (u, v) streamlines in the range $0 < z/D < 6.3$ (8.5, respectively) for the baseline wake (interaction wake, respectively). In practice, circular streamline patterns were approximated by circles, whose average geometrical center was used to locate the

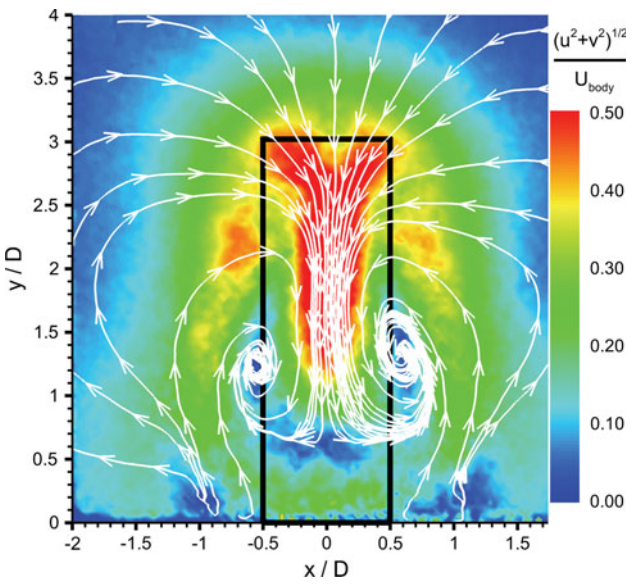

Fig. 6 Cross-sectional (x, y) distribution of the normalized phase-averaged mean velocity with streamlines overlaid at $z/D = 1.49$ for the baseline wake flow, showing the free-end vortex pair and associated downwash (adapted from Poussou 2008)

corresponding vortex cores. Since spatial and temporal coordinates were known at each z/D plane, vortex trajectory could be plotted in cross-sectional and longitudinal planes.

The cross-sectional (x, y) vortex trajectory is plotted in Fig. 7. In the case of the baseline flow (without ventilation), the vortex pair originates near the free-end corners and descends vertically down to $y/D \approx 1$, entraining ambient fluid from the free-end and lateral sides into a recirculation region formed downstream of the body (Poussou 2008). As the vortex pair approaches lower elevations ($y/D < 1$), ground effects force vortices to convect laterally in the x-direction, where they eventually dissipate as the body moves away. The trajectories are not perfectly symmetric with respect to $x/D = 0$ due to a strong sensitivity of the low-velocity ambient flow to boundary conditions, in particular the ventilation inlet diffusers. The (x, y) vortex trajectory is found to follow a hyperbola of the

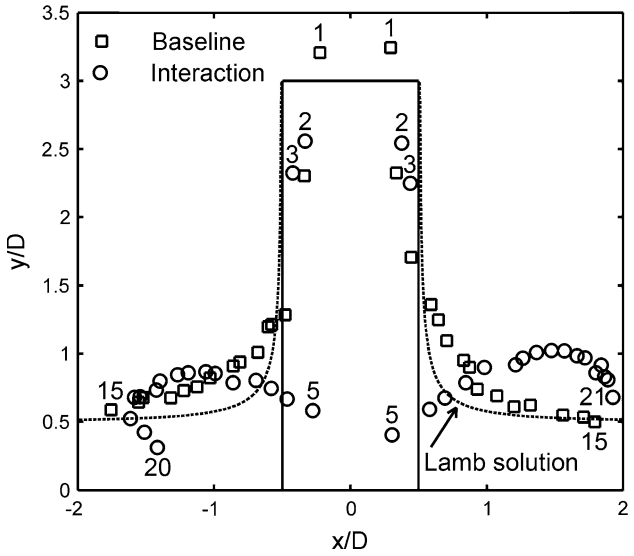

Fig. 7 Phase-averaged trajectory of the vortex core centers in (x, y) cross-sectional planes, including Lamb's inviscid solution for the baseline case. Datum numbers are frame numbers, increasing with increasing z/D

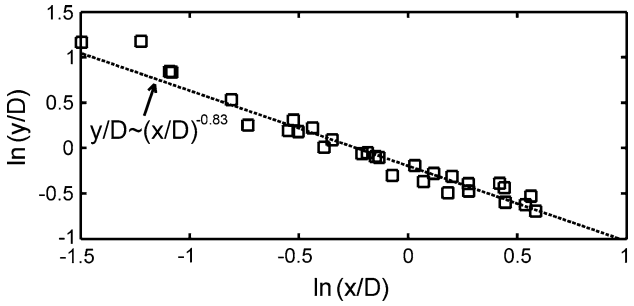

Fig. 8 Hyperbolic fit of the vortex core trajectory in (x, y) plane for the baseline case

form $y/D \propto (x/D)^{-0.83}$, as shown in Fig. 8, by fitting logarithmic quantities of x/D and y/D with a linear regression ($R^2 = 0.95$). This hyperbolic behavior suggests that transport of contaminant emitted in the upper body region is entrained at early stages of wake development corresponding to $z/D < 2$. From an analytical point of view, these trajectories can be compared to those followed by the classical, two-dimensional Lamb dipole calculated for an inviscid fluid bounded by a solid wall (Saffman 1979). If vortices are initially separated by a distance $2x_0$, the Lamb's solution takes the form $x_0^2(x^2 + y^2) = x^2y^2$. as indicated by the dashed line in Fig. 7 for $x_0 = 0.5$. The qualitative trend compares favorably with the present baseline data (square symbols). Note that large deviations observed for $0.5 < |x/D| < 1$ can be attributed to viscosity, turbulence and three-dimensional effects. Moreover, entrainment of ambient fluid into the wake from the sides of the body results in lateral spreading of the wake and therefore, conservation of mass produces deviation from Lamb's solution as y/D reaches values lower than 1. Both flows are in remarkably favorable agreement for $|x/D| > 1.5$. Saffman (1991) showed that in a viscous fluid, a boundary layer forms near the wall and may separate, inducing vortex rebound. Such flow phenomena could not be observed within the limited field of view of the present experiment. In the case of the interaction flow (with ventilation), Fig. 7 shows that the vortex pair follows the same initial trajectory as the baseline vortices (interaction data points 2 and 3); however, vortices in the wake are observed to reorganize due to strong three-dimensionality and the vortex pair consistently follows a different path after data point 5. Note that data point 4 is not present because the vortex pair was not visible in this plane. Such deviation can be explained by the upwash flow from both lateral sides contributed by the ventilation flow: as the body moves away, lateral convection of the vortex pair in the x-direction is prevented by the opposing ventilation flow and vortices are confined within $x/D < 2$ even as the body is far away at $z/D = 8.5$. For reference, the cross-sectional distribution of the baseline ventilation flow without wake interaction is illustrated in Fig. 9, as reported in Poussou (2008). Velocity field data show two large counter-rotating vortical cells across the cabin, with vortex cores at slightly different vertical locations due to the sensitivity of the ambient flow to boundary conditions. As the flow circulates from the diffuser to the floor, a stagnation region is formed near $x/D = 0$ and extends vertically up to $y/D = 0.8$, which would correspond approximately to the lower third of the moving body height (i.e. legs). This velocity field is in qualitative agreement with Mazumdar and Chen (2008) for a Boeing 767 ventilated cabin.

The longitudinal (y, z) vortex trajectory is plotted in Fig. 10 and shows the y- vortex location averaged over

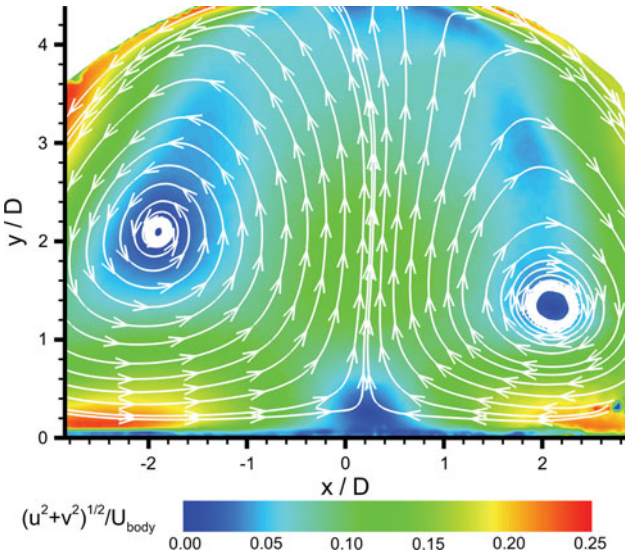

Fig. 9 Cross-sectional (x, y) distribution of the normalized mean velocity with streamlines overlaid for the baseline ventilation flow in the cabin, showing the ambient recirculation pattern (adapted from Poussou 2008)

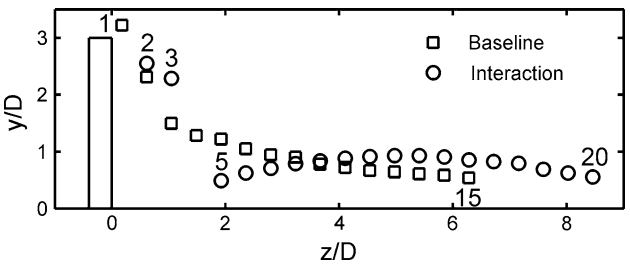

Fig. 10 Phase-averaged trajectory of the vortex core centers in (y, z) longitudinal planes. Datum numbers are frame numbers, increasing with increasing z/D

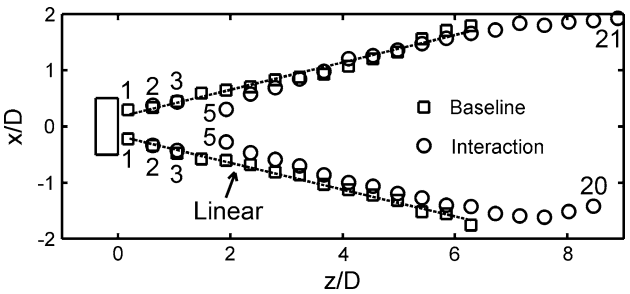

Fig. 11 Phase-averaged trajectory of the vortex core centers in (x, z) horizontal planes, including a linear regression for the baseline case. Datum numbers are frame numbers, increasing with increasing z/D

both sides of the cabin. The data show that the ventilation flow lifts the vortex pair from $y/D = 0.5$ to 1 above vertical elevations measured in the absence of ventilation. This observation suggests that contaminant in the wake remains

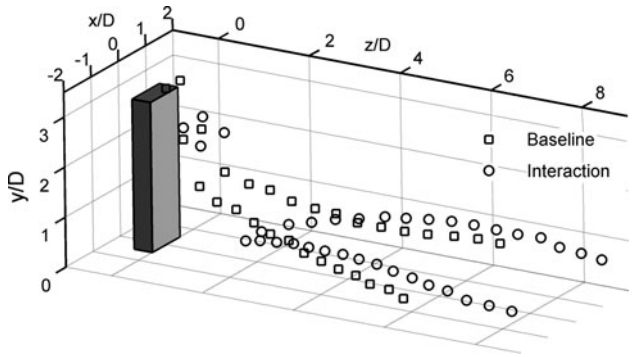

Fig. 12 Phase-averaged trajectory of the vortex core centers in (x, y, z) space

at high vertical location due to the effect of the recirculating ventilation pattern.

Lateral convection of the vortex pair is plotted in horizontal (x, z) planes, as shown in Figs. 11 and 12. In the absence of ventilation, lateral spreading is well approximated by linear regressions up to $z/D = 6$, with a functional correlation of the form $x = 0.24z + 0.17$ ($R^2 = 0.98$). The ventilation flow is observed to clearly limit lateral convection to values $|x/D| < 2$. Vortex reorganization takes place between interaction data points 3 and 5. A secondary vortex pair forms near the floor as the free-end downwash weakens due to the opposing effect of the ventilation flow.

4.2 Scalar transport in the wake

Flow visualization results confirm the flow dynamics suggested by the kinematic evolution of the vortex pair, as well as velocity field data (Poussou 2008). Cross-sectional flow visualization is shown for the baseline wake in Fig. 13. Dye is initially emitted uniformly on each side, with a minor amount convected above the free-end from the corners. Early in flow development, dye migrates preferentially to the upper body region (frame 2) from the lateral sides. As the downwash flow develops (frame 3), the vortex pair is observed to spread the wake at its midsection, and vortices eventually impinge the floor (frame 6). Sufficiently far downstream of the body (frame 10), a narrow region of unmixed dye is observed to persist at constant elevation $y/D \approx 1$. Recirculation in the wake is visible in the central plane ($x/D = 0$). Figure 14 shows large-scale elongated dye regions transported in the wake in the forward direction at an angle with the horizontal of approximately 45°. This is consistent with instantaneous PIV velocity fields showing high velocity entrainment into the wake at same angle, which results from the combination of downward convection of the counter-rotating vortex pair with forward motion. For an observer fixed on the floor, the

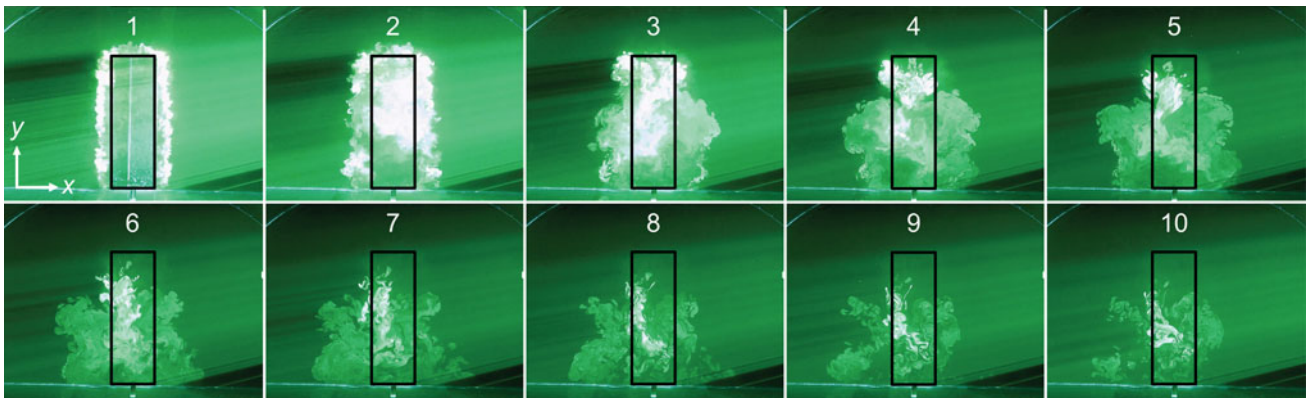

Fig. 13 Flow visualization of the baseline wake in (x, y) cross-sectional plane. Dye injection starts at a distance $z = d_2 - 10D$ from the origin. Inset numbers are frame numbers, increasing with increasing z/D

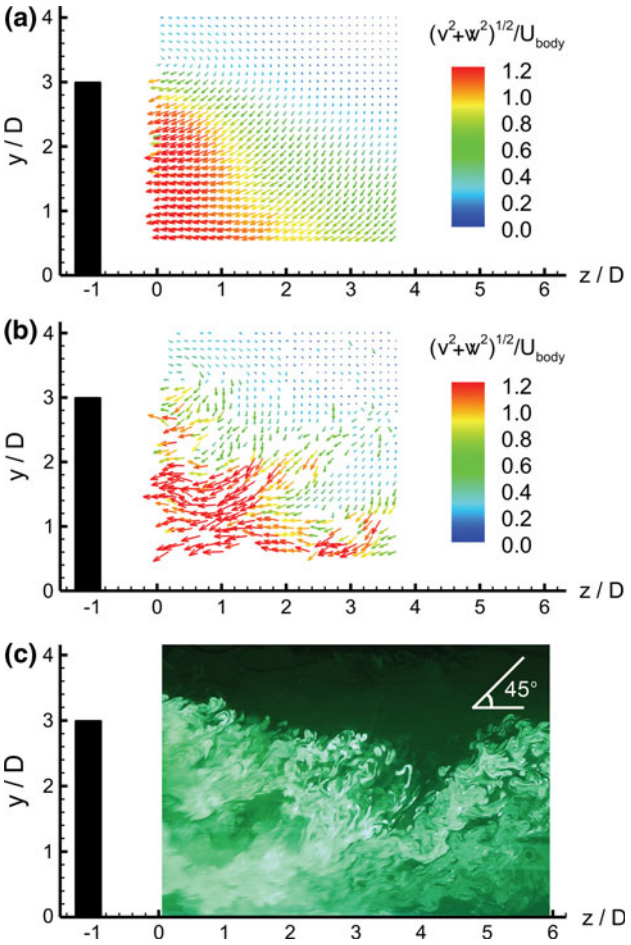

Fig. 14 Longitudinal view in (y, z) plane of the near-wake baseline flow at $z/D = 0.87$, showing **a** mean velocity field, **b** instantaneous velocity field, and **c** instantaneous flow visualization

pattern resembles bands of dye following the body and oriented from high to low elevations in the forward direction, which is contrary to the intuitive view of high to low elevations in the backward direction in the case of wakes behind stationary objects. These patterns correspond to intermittent structures mentioned by Edge et al. (2005) in real-scale smoke visualization behind a person walking.

In the interaction case (Fig. 15), dye is found to be initially distributed less uniformly in the vertical direction than in the baseline case (frame 1) due to the sweeping effect of the ventilation flow near the floor. Dye is observed at lower concentrations in the lower section ($y/D < 1.5$). At frame 1, dye has already started to convect to the central region near $x/D = 0$. The upper region ($y/D > 1.5$) does not show evidence of strong downwash from frames 2 to 4, unlike the baseline flow. Instead, dye remains at the same horizontal and vertical location until frame 10, which corresponds to a downstream distance $z/D = 4$. Therefore, flow visualization suggests that entrainment in the forward direction is inhibited because of the significantly weaker pair of counter-rotating vortices.

Cross-sectional observations are confirmed by longitudinal flow visualization, as shown in Fig. 16. The elongated, inclined regions of concentrated dye observed in the baseline wake at a 45° angle are replaced by regions qualitatively showing less inclination, i.e. more vertical. As they form, they are not transported in the forward direction but instead, they are found to remain stationary at constant z/D locations, until they are completely mixed by the ventilation flow far downstream of the body ($z/D > 10$). Dye is also visible at higher vertical y/D elevation along the entire length of the wake, which confirms that the ventilation flow lifts the wake and its contaminant.

Although quantitative PLIF-based techniques have been developed to measure the concentration of scalar tracers in complex flows (Koochesfahani and Dimotakis 1986), such study was beyond the scope of the present work to investigate the relative variation of contaminant distribution. Instead, the temporal evolution of contaminant was obtained by phase-averaging cross-sectional PLIF images (30 for the baseline case, 50 for the interaction case). The

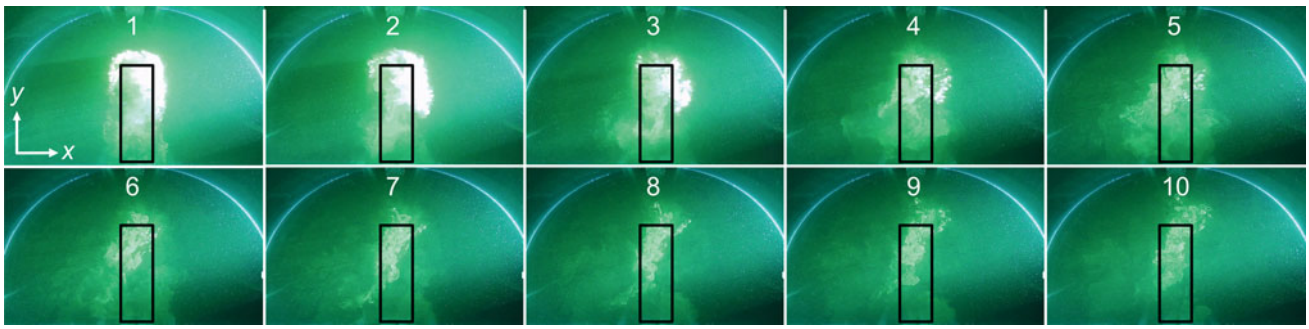

Fig. 15 Flow visualization of the interaction wake in (x, y) cross-sectional plane. Dye injection starts at a distance $z = d_2 - 10D$ from the origin. Inset numbers are frame numbers, increasing with increasing z/D

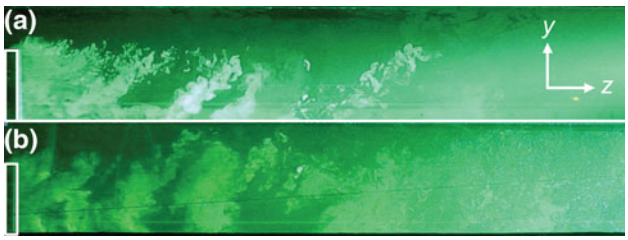

Fig. 16 Instantaneous flow visualization in (y, z) longitudinal planes of **a** baseline, and **b** interaction wakes

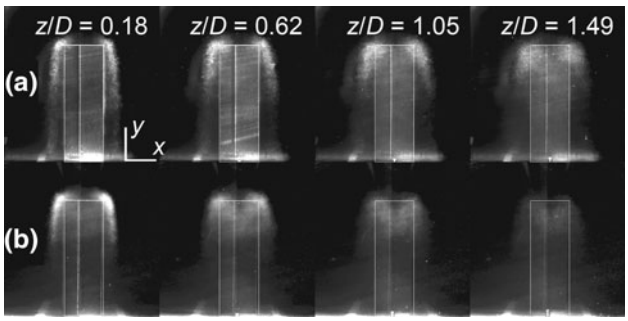

Fig. 17 Streamwise evolution of phase-averaged (x, y) cross-sectional PLIF images of **a** baseline and **b** interaction wakes at various z/D distances

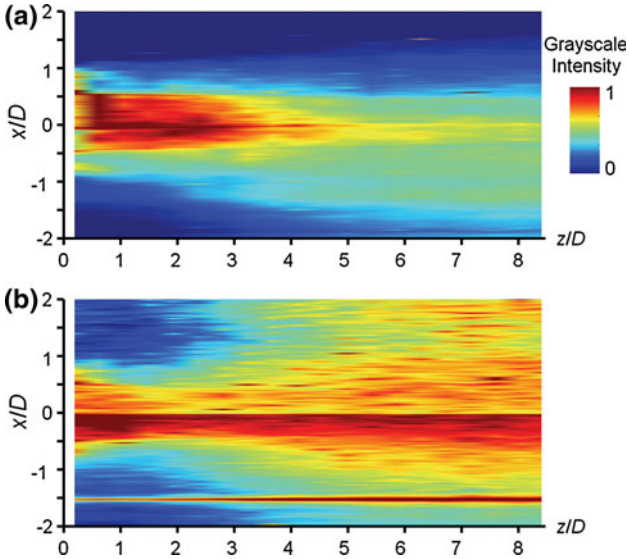

Fig. 18 Streamwise evolution of phase-averaged (x, z) horizontal PLIF intensity levels of **a** baseline and **b** interaction wakes at $y/D = 1.5$

streamwise evolution of scalar distribution in the near-wake region ($z/D < 1.5$) is shown in Fig. 17, where relative decay is more strongly observed in the interaction case. Dye was injected uniformly along the vertical edges of the body in both flows and scalar distributions at $z/D = 0.18$ shows that dye convected consistently toward the free-end corners where the counter-rotating vortices form, which is consistent with incipient wake formation mechanisms identical in both cases. However, dye was observed to decay in the near-wake more rapidly with ventilation. Grayscale intensity levels were further averaged in each cross-sectional (x, y) plane over 1 mm^2 square interrogation zones and ensemble-averaged. For this purpose, grayscale pixel intensities in each (x, y) image were normalized by the minimum (in the background) and the maximum (in the shear layer) intensity levels measured at $z/D = 0.18$ to permit relative comparison of successive z/D images. The resulting (x, z) streamwise evolution of scalar distribution is shown at $y/D = 1.5$ in Fig. 18 and $y/D = 2.25$ in Fig. 19, where the longitudinal extent of the wake is visibly reduced by the ventilation effect. Note that in the interaction case, the line observed at $x/D \approx -1.5$ is independent of the experiment and was caused by light reflecting on an undesired object in the background outside the water tank. Significant deviation from the baseline flow can be observed due to ventilation. In the baseline case, lateral spread of dye is limited to $-1 < x/D < 1$, whereas in the interaction flow, dye is observed to extend beyond $|x/D| = 1$, i.e. to the entire cabin cross-section. This suggests that the downwash is inhibited by the upward ventilation and contaminant mixes with the ambient recirculating flow instead of convecting to the ground plane.

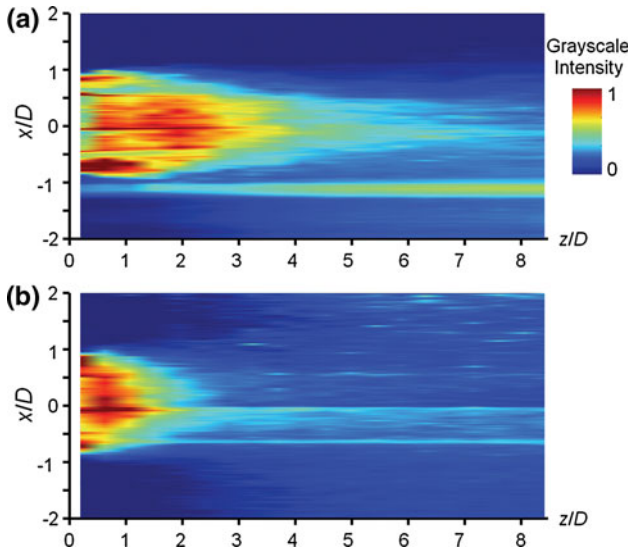

Fig. 19 Streamwise evolution of phase-averaged (x, z) horizontal PLIF intensity levels of **a** baseline and **b** interaction wakes at $y/D = 2.25$

5 Discussion

The main effect of the ventilation flow is to inhibit the downwash by altering the development of the pair of counter-rotating vortices forming near the free-end of the body. In the near-wake region ($z/D < 1$), the corner vortices from the shoulders induce downward flow and are observed to form at earlier flow stages than in the baseline case. Their formation is not significantly affected by the ventilation because forced convection due to the wake is greater than forced convection due to the ventilation flow at this elevation. They quickly dissipate before reaching the body mid-height (i.e. lower abdomen). In the meantime, strong recirculation flow is produced in the forward direction along the centerline at mid-section and is accompanied by entrainment of ambient fluid through the lateral shear layers. By conservation of mass, intrusion of fluid from the free-end results in a reorganization of the wake vortical structure and a secondary pair of counter-rotating vortices forms near the floor, which spreads the base of the wake. As studied in further details by Poussou (2008) through velocity field measurements in the near wake between $z/D = 0$ and 5, the corner vortex pair (primary) and the base vortex pair (secondary) do not coexist simultaneously because the corner vortices form, reorganize, and weaken before the base vortices are formed. As a result, the downwash from the free-end is not completely convected to floor level, which suggests that a significant fraction of contaminant entrained from the upper body region by the corner vortices remains confined above mid-height. From an observer fixed on the floor, the longitudinal extent of the wake is reduced and the ventilation flow 'freezes' transport of contaminant in the forward direction due to the shorter duration of the free-end vortices. It follows that elongated structures that are typically observed at an angle with the horizontal in the baseline flow are replaced by quasi-vertical structures because free-end vortices do not convect to the floor while being entrained forward. The effect of the ventilation is to decouple downwash and forward entrainment by breaking the development of the free-end vortices, as further shown by (x, z) velocity field data in Poussou (2008). In the far wake region ($z/D > 10$), contaminant present above mid-height is recirculated until being eventually mixed totally in the cabin by the ventilation flow. In summary, the interaction between the ventilation flow and the wake from the moving body opposes the downwash mechanism. Such ventilation pattern promotes the suspension of contaminant emitted near the free-end at elevations remaining above middle body section instead of convecting contaminant to floor level. As a consequence, aerosols emitted above mid-body height would tend to remain at vertical elevations corresponding to seated passengers breathing levels, and thus promote onboard contamination.

The present study considered an idealized representation of a human walking in a cabin, in which the ventilation flow was shown to affect wake development. Such ventilation effects and higher vertical mixing may become insignificant as the body speed is increased. Additionally, buoyancy effects contributed by real passengers may alter the fate of contaminants transported in the wake depending on their walking speed, potentially promoting contaminant migration to higher vertical elevations. Finally, the flow around an idealized human body represented as a parallelepiped bluff body has been shown to be sensitive to finer scale geometrical details (Edge et al. 2005), which may further affect wake development and mixing in the presence of ventilation.

6 Summary and conclusions

The interaction between a flow recirculating in a semi-circular enclosure ($Re_h = 500$) and the wake behind a bluff body moving at constant speed ($Re_D = 9{,}600$) was investigated experimentally in the context of dispersion of contaminants in ventilated aircraft cabins. The objective of the study was to identify fluid flow mechanisms governing the migration of a scalar contaminant in the wake of a human moving through the cabin ventilation flow typical of a Boeing 767-300 aircraft. The upward recirculating ventilation flow was found to suppress the downwash from the moving passenger by altering the development of a pair of counter-rotating vortices produced near the free-end of the body. In the near-wake region ($z/D < 1$), these vortices

were observed to form earlier during wake development than in the absence of recirculating flow. However, the vortex pair dissipated prior reaching mid-body height while strong recirculating flow was produced in the forward direction along the centerline at mid-section. This strongly three-dimensional flow accentuated longitudinal recirculation in the near-wake region. Ambient fluid was more strongly entrained into the wake through the lateral shear layers. Intrusion of fluid from the free-end was reinforced by the formation of a secondary pair of counter-rotating vortices near the floor, which spread the base of the wake in the lateral direction. The corner vortex pair and the base vortex pair did not coexist simultaneously because the corner vortices formed, reorganized, and dissipated before the base vortices formed. Alteration of the downwash prevented the downward convection of contaminant to the floor, which therefore remained in suspension at higher vertical elevations before being mixed and spread within the cabin cross-section. In summary, the upward recirculating flow was found to decouple the downwash mechanism from forward entrainment by opposing the convection of the free-end vortices. The flow interaction between a human wake and particular ventilation patterns has potential to increase contaminant dispersion in the cabin and extend the contamination zone to multiple seat rows along a cabin length, which would promote transmission of airborne pathogens and adversely affect the performance of the ventilation flow. Specific details of the flow interactions and contaminant dispersion will depend on the type of aircraft, seating configuration and ventilation scheme.

Acknowledgments This project was funded by the U.S. Federal Aviation Administration (FAA) Office of Aerospace Medicine through the National Air Transportation Center of Excellence for Research in the Intermodal Transport Environment under Cooperative Agreement 07-C-RITE-PU. Although the FAA has sponsored this project, it neither endorses nor rejects the findings of this research. The presentation of this information is in the interest of invoking technical comment on the results and conclusions of the research.

References

Aboosaidi F, Warfield MJ, Choudhury D (1991) Computational fluid dynamics applications in airplane cabin ventilation system design. In: Proceedings of the international conference on environmental systems, society of automotive engineers, pp 249–258

Afgan I, Moulinec C, Prosser R, Laurence D (2007) Large eddy simulation of turbulent flow for wall mounted cantilever cylinders of aspect ratio 6 to 10. Int J Heat Fluid Fl 28(4):561–574

Baker AJ, Ericson SC, Orzechowski JA, Wong KL, Garner RP (2006) Aircraft passenger cabin ECS-generated ventilation velocity and mass transport CFD simulation: velocity field validation. J IEST 49(2):51–83

Baker AJ, Ericson SC, Wong KL, Garner RP (2008) Aircraft passenger cabin ECS-generated ventilation velocity and mass transport CFD simulation: mass transport validation exercise. J IEST 51(1):90–113

Bosbach J, Pennecot J, Wagner C, Raffel M, Lerche T, Repp S (2006) Experimental and numerical simulations of turbulent ventilation in aircraft cabins. Energy 31(5):694–705

Budwig R (1994) Refractive index matching methods for liquid flow investigations. Exp Fluids 17(5):350–355

Chen QY, Lee K, Mazumdar S, Poussou SB, Wang L, Wang M, Zhang Z (2010) Ventilation performance prediction for buildings: model assessment. Build Environ 45(2):295–303

Chen SC, Chang CF, Liao CM (2006) Predictive models of control strategies involved in containing indoor airborne infections. Indoor Air 16(6):469–481

Choi JI, Edwards JR (2008) Large eddy simulation and zonal modeling of human-induced contaminant transport. Indoor Air 18(3):233–249

Craven BA, Settles GS (2006) A computational and experimental investigation of the human thermal plume. J Fluids Eng 128(6): 1251–1258

Dechow M, Sohn H, Steinhanses J (1997) Concentrations of selected contaminants in cabin air of Airbus aircrafts. Chemosphere 35(1–2):21–31

Doligalski TL, Smith CR, Walker JDA (1994) Vortex interactions with walls. Annu Rev Fluid Mech 26:573–616

Donnert GD, Kappler M, Rodi W (2007) Measurement of tracer concentration in the flow around finite-height cylinders. J Turbul 8(33):1–18

Edge BA, Paterson EG, Settles GS (2005) Computational study of the wake and contaminant transport of a walking human. J Fluids Eng 127(5):967–977

Farivar D (1981) Turbulent uniform flow around cylinders of finite length. AIAA J 19(3):275–281

Flynn MR, Eisner AD (2004) Verification and validation studies of the time-averaged velocity field in the very near-wake of a finite elliptical cylinder. Fluid Dyn Res 34(4):273–288

Fröhlich J, Rodi W (2004) LES of the flow around a circular cylinder of finite height. Int J Heat Fluid Fl 25(3):537–548

Gao NP, Niu JL (2007) Modeling particle dispersion and deposition in indoor environments. Atmos Environ 41(18):3862–3876

Gao NP, Niu JL (2008) Personalized ventilation for commercial aircraft cabins. J Aircraft 45(2):508–512

Garner RP, Wong KL, Ericson SC, Baker AJ, Orzechowski JA (2004) CFD validation for contaminant transport in aircraft cabin ventilation. Report DOT/FAA/AM-04/7, Office of Aerospace Medicine, U.S. Department of Transportation, Washington, DC

Huber AH, Arya SP, Rajala SA, Borek JW (1991) Preliminary studies of video images of smoke dispersion in the near wake of a model building. Atmos Environ 25A(7):1199–1209

Karasso PS, Mungal MG (1997) PLIF measurements in aqueous flows using the Nd:YAG laser. Exp Fluids 23(5):382–387

Kawamura T, Hiwada M, Hibino T, Mabuchi I, Kumada M (1984) Flow around a finite circular cylinder on a flat plate (cylinder height greater than turbulent boundary layer thickness). B JSME 27(232):2142–2151

Kenyon TA, Valway SE, Ihle WW, Onorato IM, Castro KG (1996) Transmission of multidrug-resistant mycobacterium tuberculosis during a long airplane flight. New Engl J Med 334(15):933–938

Kim T, Flynn MR (1991) Air-flow pattern around a worker in a uniform freestream. Am Ind Hyg Assoc J 52(7):287–296

Kolar V, Lyn DA, Rodi W (1997) Ensemble-averaged measurements in the turbulent near wake of two side-by-side square cylinders. J Fluid Mech 346:201–237

Koochesfahani MM, Dimotakis PE (1986) Mixing and chemical reactions in a turbulent liquid mixing layer. J Fluid Mech 170: 83–112

Kühn M, Bosbach J, Wagner C (2008) Experimental parametric study of forced and mixed convection in a passenger aircraft cabin mock-up. Build Environ 44(5):961–970

Kulmala I, Saamanen A, Enbom S (1996) The effect of contaminant source location on worker exposure in the near-wake region. Ann Occup Hyg 40(5):511–523

Lai ACK, Wang K, Chen FZ (2008) Experimental and numerical study on particle distribution in a two-zone chamber. Atmos Environ 42(8):1717–1726

Lakehal D, Rodi W (1997) Calculation of the flow past a surface-mounted cube with two-layer turbulence models. J Wind Eng Ind Aerodyn 67–68:65–78

Liou TM, Chen SH, Hwang PW (2002) Large eddy simulation of turbulent wake behind a square cylinder with a nearby wall. J Fluids Eng 124(1):81–90

Liu W, Mazumdar S, Zhang Z, Poussou SB, Liu J, Lin CH, Chen Q (2012) State-of-the-art methods for studying air distributions in commercial airliner cabins. Build Environ 47:5–12

Lübcke H, Schmidt S, Rung T, Thiele F (2001) Comparison of LES and RANS in bluff-body flows. J Wind Eng Ind Aerodyn 89(14–15):1471–1485

Mangili A, Gendreau MA (2005) Transmission of infectious diseases during commercial air travel. Lancet 365(9463):989–996

Martinuzzi R, Tropea C (1993) The flow around surface-mounted, prismatic obstacles placed in a fully developed channel flow. J Fluids Eng 115(85):85–92

Mazumdar S, Chen Q (2008) Influence of cabin conditions on placement and response of contaminant detection sensors in a commercial aircraft. J Environ Monit 10(1):71–81

Mazumdar S, Poussou SB, Lin CH, Isukapalli SS, Plesniak MW, Chen Q (2011) Impact of scaling and body movement on contaminant transport in airliner cabins. J Environ Monit 45(33): 6019–6028

McKernan LT, Wallingford KM, Hein MJ, Burge H, Rogers CA, Herrick R (2008) Monitoring microbial populations on wide-body commercial passenger aircraft. Ann Occup Hyg 52(2):139–149

Mizuno T, Warfield MJ (1992) Development of three-dimensional thermal airflow analysis computer program and verification test. ASHRAE J 98(2):329–338

Mo H, Hosni MH, Jones BW (2003) Application of particle image velocimetry for the measurement of the airflow characteristics in an aircraft cabin. ASHRAE J 109(1):101–110

Moffat RJ (1988) Describing the uncertainties in experimental results. Exp Therm Fluid Sci 1(1):3–17

Moser RM, Bender TR, Margolis HS, Noble GR, Kendal AP, Ritter DG (1979) An outbreak of influenza aboard a commercial airliner. Am J Epidemiol 110(1):1–6

Müller RHG, Scherer T, Rötger T, Schaumann O, Markwart M (1997) Large body aircraft cabin A/C flow measurement by helium bubble tracking. J Flow Vis Image Proc 4:295–306

Murakami S, Zeng J, Hayashi T (1999) CFD analysis of wind environment around a human body. J Wind Eng Ind Aerodyn 83:393–408

Nagda NL, Koontz MD, Konheim AG, Hammond SK (1992) Measurement of cabin air quality aboard commercial airliners. Atmos Environ 26A(12):2203–2210

National Research Council (2002) The airliner cabin environment and the health of passengers and crew. National Academy Press, Washington, DC

Okamoto S, Sunabashiri Y (1992) Vortex shedding from a circular cylinder of finite length placed on a ground plane. J Fluids Eng 114(4):512–521

Okamoto T, Yagita M (1973) The experimental investigation on the flow past a circular cylinder of finite length. B JSME 16(95): 805–814

Olsen SJ, Chang HL, Cheung TYY, Tang AFY, Fisk TL, Ooi SPL, Kuo HW, Jiang DDS, Chen KT, Lando J, Hsu KH, Chen TJ, Dowell SF (2003) Transmission of severe acute respiratory syndrome on aircraft. New Engl J Med 349(25):2416–2422

Park CW, Lee SJ (2000) Free end effects on the near wake flow structure behind a finite circular cylinder. J Wind Eng Ind Aerodyn 88(2–3):231–246

Park CW, Lee SJ (2002) Flow structure around a finite circular cylinder embedded in various atmospheric boundary layers. Fluid Dyn Res 30(4):197–215

Park CW, Lee SJ (2004) Effects of free-end corner shape on flow structure around a finite cylinder. J Fluid Struct 19(2):141–158

Poussou SB (2008) Experimental investigation of airborne contaminant transport by a human wake moving in a ventilated aircraft cabin. PhD thesis, Purdue University, West Lafayette, Indiana, USA

Poussou SB, Mazumdar S, Plesniak MW, Sojka PE, Chen Q (2010) Flow and contaminant transport in an airliner cabin induced by a moving body: model experiments and CFD predictions. Atmos Environ 44(24):2830–2839

Richmond-Bryant J, Eisner AD, Flynn MR (2006) Considerations for modeling particle entrainment into the wake of a circular cylinder. Aerosol Sci Tech 40(1):42–51

Roshko A (1993) Perspectives on bluff body aerodynamics. J Wind Eng Ind Aerodyn 49(1–3):79–100

Saffman PG (1979) The approach of a vortex pair to a plane surface in inviscid fluid. J Fluid Mech 92:497–503

Saffman PG (1991) Approach of a vortex pair to a rigid free surface in viscous fluid. Phys Fluids A3(5):984–985

Saha AK, Biswas G, Muralidhar K (2001) Two-dimensional study of the turbulent wake behind a square cylinder subject to uniform shear. J Fluids Eng 123(3):595–603

Sakamoto H, Arie M (1983) Vortex shedding from a rectangular prism and a circular cylinder placed vertically in a turbulent boundary layer. J Fluid Mech 126:147–165

Singh A, Hosni MH, Horstman RH (2002) Numerical simulation of airflow in an aircraft cabin section. ASHRAE J 108(1):1005–1013

Slaouti A, Gerrard JH (1981) An experimental investigation of the end effects on the wake of a circular cylinder towed through water at low Reynolds numbers. J Fluid Mech 112:297–314

Song CCS, He J (1993) Computation of wind flow around a tall building and the large-scale vortex structure. J Wind Eng Ind Aerodyn 46–47:219–228

Spengler JD, Wilson DG (2003) Air quality in aircraft. P I Mech Eng E-J Pro 217(E4):323–335

Sumner D, Heseltine JL, Dansereau OJP (2004) Wake structure of a finite circular cylinder of small aspect ratio. Exp Fluids 37(5): 720–730

Sun Y, Zhang Y, Wang A, Topmiller JL, Bennett JS (2005) Experimental characterization of airflows in aircraft cabins, part I: experimental system and measurement procedure. ASHRAE J 111(2):45–52

Tanaka S, Murata S (1999) An investigation of the wake structure and aerodynamic characteristics of a finite circular cylinder. B JSME 42(2):178–187

Taniguchi S, Sakamoto H, Arie M (1981) Flow around a circular cylinder vertically mounted in a turbulent boundary layer. B JSME 24(193):1130–1136

Taniguchi S, Sakamoto H, Arie M (1981) Flow around circular cylinders of finite height placed vertically in turbulent boundary layers. B JSME 24(187):37–44

Thomas RH, Schetz JA, Pelletier DH (1991) Three-dimensional finite element method analysis of turbulent flow over self-propelled slender bodies. J Propul Power 7(2):281–287

Wang A, Zhang Y, Sun Y (2005) Streak recognition for a three-dimensional volumetric particle tracking velocimetry system. ASHRAE J 111(2):476–484

Wang A, Zhang Y, Topmiller JL, Bennett JS, Dunn KH (2006) Tracer study of airborne disease transmission in an aircraft cabin mock-up. ASHRAE J 112(2):697–705

Wang A, Zhang Y, Sun Y, Wang X (2008) Experimental study of ventilation effectiveness and air velocity distribution in an aircraft cabin mockup. Build Environ 43(3):337–343

Wang PD (2000) Two-step tuberculin testing of passengers and crew on a commercial airplane. Am J Infect Control 28(3):233–238

Wick RL, Irvine LA (1995) The microbiological composition of airliner cabin air. Aviat Space Environ Med 66(3):220–224

Williamson CHK (1996) Vortex dynamics in the cylinder wake. Annu Rev Fluid Mech 28:477–539

Wolochuk MC, Plesniak MW, Braun JE (1996) The effects of turbulence and unsteadiness on vortex shedding from sharp-edged bluff bodies. J Fluids Eng 118(1):18–25

Yan W, Zhang Y, Sun Y, Li D (2009) Experimental and CFD study of unsteady airborne pollutant transport within an aircraft cabin mock-up. Build Environ 44(1):34–43

Zhang T, Chen Q (2007) Identification of contaminant sources in enclosed spaces by a single sensor. Indoor Air 17(6):439–449

Zhang T, Chen Q (2007) Novel air distribution systems for commercial aircraft cabins. Build Environ 42(4):1675–1684

Zhang T, Chen Q, Lin CH (2007) Optimal sensor placement for airborne contaminant detection in an aircraft cabin. HVAC&R Res 13(5):683–696

Zhang Y, Sun Y, Wang A, Topmiller JL, Bennett JS (2005) Experimental characterization of airflows in aircraft cabins, part II: results and research recommendations. ASHRAE J 111(2): 53–59

Zhang Z, Chen X, Mazumdar S, Zhang T, Chen Q (2009) Experimental and numerical investigation of airflow and contaminant transport in an airliner cabin mockup. Build Environ 44(1):85–94

Zitter JN, Mazonson PD, Miller DP, Hulley SB, Balmes JR (2002) Aircraft cabin air recirculation and symptoms of the common cold. JAMA J Am Med Assoc 288(4):483–486